Ferroelectric order stability in the $Bi_{1-x}Pb_xFeO_3$ solid solution

J. Chaigneau,[1] R. Haumont,[2] and J. M. Kiat[1,3]
[1]*Laboratoire Structures, Propriétés et Modélisation des Solides, Ecole Centrale Paris, CNRS UMR 8580, Grande Voie des Vignes, 92295 Châtenay-Malabry Cedex, France*
[2]*Laboratoire de Physico-Chimie de l'Etat Solide, ICMMO, CNRS UMR 8182, Université Paris XI, 91405 Orsay, France*
[3]*Laboratoire Léon Brillouin, CE Saclay, CNRS UMR 12, 91991 Gif-Sur-Yvette Cedex, France*
(Received 5 March 2009; revised manuscript received 9 July 2009; published 16 November 2009)

Ferroelectric properties of $Bi_{1-x}Pb_xFeO_3$, through a structural approach, by structural Rietveld refinement and x-ray diffraction versus temperature have been carried out. This study allows us to draw a phase diagram for the system $Bi_{1-x}Pb_xFeO_3$. Although lead atom gets a lone pair and is commonly understood as having a "ferroelectric" character, we report in this paper that adding of lead atom in the Bi subsystem of $BiFeO_3$, destroys the long-range FE order induced by Bi lone pairs on contrary, and progressively breaks the ferroelectric ordering up to the point where the structure becomes cubic on average. The decreasing of T_C with increasing Pb content also confirms that adding of Pb atoms destabilizes the ferroelectric rhombohedral order and stabilizes the cubic phase via a complex texture of mixed phases, occurring at a local scale.

DOI: 10.1103/PhysRevB.80.184107 PACS number(s): 61.05.C−, 77.80.Bh

I. INTRODUCTION

Multiferroic materials that can simultaneously display ferroelectric and magnetic ordering[1] attract more and more interest since the last few years. The fundamental understanding and experimental observation of the possible coupling between ferroelectric and magnetic order is currently among the most challenging topics in the solid-sate physics.[2–5] Among multiferroics, the bismuth ferrite $BiFeO_3$ (BFO) is considered as the "prototype," probably the most studied, as it constitutes the most promising candidates for realizing multiferroic spintronics devices.[6] This perovskite presents a coexistence of both ferroelectric and antiferromagnetic order up to unusually high temperatures, namely, above the room temperature. In bulk material, this "robust" $BiFeO_3$ has an antiferromagnet (AFM) Néel temperature $T_N \sim 370$ °C,[7] and a ferroelectric Curie temperature $T_C \sim 820$ °C.[8] At room temperature, $BiFeO_3$ crystallizes in a highly distorted rhombohedral perovskite, which belongs to the space group $R3c$.[7,9] With respect to the ideal cubic $Pm\bar{3}m$ structure of perovskite-type oxides, the rhombohedral structure can be represented by an antiphase tilt of the adjacent FeO_6 octahedra ($a^-a^-a^-$ in Glazer's notation[10]) and displacement of both the Fe^{3+} and Bi^{3+} cations from their centrosymmetric position along the pseudocubic $[111]_{pc}$ direction. The mechanism for the ferroelectricity essentially comes from the long-range ordering of dipolar moments on Bi site, in relation with the existence of Bi lone pair and hybridization between Bi $6s$ and O $2p$.[11]

In order to enhance its ferroelectric and magnetic properties, many authors have already reported chemical substitution on the A and/or the B site of $BiFeO_3$. By changing the local chemical composition of the structure (i.e., the content of polar/magnetic cations), it is possible to modify the global physical properties of the multiferroic compound and thus to acquire a better understanding of the magnetic/polar coupling which in turn will guide synthesis of novel and greatly improved materials. The goal of such chemical substitution in $BiFeO_3$ is mainly to alter the Fe environment by (i) modifying the charge of Fe^{3+}, as mechanisms of charge compensation are expected if A and/or B cations have a charge different from 3, (ii) introducing oxygen vacancies, (iii) changing Fe-O length bond, and/or (iv) Fe-O-Fe angle. Consequently, all theses parameters should modify the AFM superexchange, and in some cases a breaking of the AFM order is observed toward a ferromagnetic phase. For instance, the influence on the cycloid suppression by doping (Ca, Sr, Pb, and Ba) was checked in a study carried out by Khomchenko *et al.*[12–14] whereas enhancement of magnetization was also reported in $Bi_{1-x}RE_xFeO_3$ (RE=Nd, Sm, and Tb) (Refs. 15 and 16). Also, the effect of $PbZrO_3$ doping on $BiFeO_3$ was shown to result in noticeable lattice expansion and a significant decrease in T_N.[17]

The impact of substitution on the ferroelectricity is often checked by carrying out hysteresis loop studies at room temperature. Nevertheless, electric losses and conductivity effects induced by substitutions, as well as conditions of the synthesis or sintering processes often limit the measurements. Besides, closed loops associated to switched charge versus applied voltage are nearly identical to ferroelectric hysteresis loops, and this rise questions on some reports of ferroelectricity in such compounds.[18] In the other hand, the ferroelectric character can be easily investigated by a structural Rietveld refinement which allows to determine correct space group (i.e., in particular, polar or nonpolar group), and calculate in such a case exact off-centered shifts of ions and polarization from effective charges.

Within this context, we have investigated the $Bi_{1-x}Pb_xFeO_3$ solid solution. We have chosen to substitute bismuth by lead since (i) Pb has a similar electronic structure than Bi, especially existence of a lone pair. As well known this lone pair is responsible for existence of local polar disorder which in turn influence the relaxation properties in Pb-based perosvkite morphotropic systems (PMN-PT, PSN-PT,…) (Refs. 19–23); moreover, Pb doping is an interesting way to study how the ferroelectric order takes places through Bi lone pair ordering in $BiFeO_3$, and to test its stability versus substitution and temperature; (ii) differences of charge and ionic radii between Bi^{3+} and Pb^{2+} are expected to induce

structure instabilities, thus an alteration of ferroelectric and magnetic orders. The aim of this paper is to discuss ferroelectric properties of $Bi_{1-x}Pb_xFeO_3$, through a structural approach, by structural Rietveld refinement and x-ray diffraction (XRD) versus temperature. Magnetic measurements will be presented in a further report.

II. EXPERIMENT

Powders of $Bi_{1-x}Pb_xFeO_3$ with $0 \leq x \leq 0.30$ were prepared by using the conventional solid-state reaction from the mixture of Bi_2O_3, Fe_2O_3, and PbO. Starting oxides were batched in the nominal ratio and calcined twice between 820 °C and 850 °C depending on amount of Pb doping. This low temperature prevents the lead and bismuth vaporization and the formation of second phases.[24]

Diffraction patterns from $2\theta=5°$ to 120° with a step of 0.004° were collected with a Philips X-celerator Bragg-Brentano diffractometer equipped with a Copper source (monochromatic radiation $\lambda=1.54056$ Å), from 25 °C to 1000 °C under air atmosphere by using a furnace (Anton-Paar HTK1200) with an accuracy better than 2 °C. Various temperature steps were used with small ones of 10 °C around peculiar temperatures associated with phase transitions. Structural Rietveld refinements were carried out with the XND software.[25]

III. RESULTS

A. Long-range order versus concentration

Figure 1 depicts x-ray diffraction patterns at room temperature of $Bi_{1-x}Pb_xFeO_3$ powders. It reveals that the solid solution expands up to $x=0.3$. Indeed, parasitic phase, identified as $Pb_2Fe_2O_5$ (stars in diagram), appears for $x \geq 0.3$. In contrast, lower concentrations display a pure perovskite phase $Bi_{1-x}Pb_xFeO_3$, showing a solid solution, and exhibiting well-defined diffraction peaks localized around conventional 2θ Bragg positions expected for a pseudocubic perovskite with a cell parameter closed to 4 Å. The extend of the solid solution is probably limited by the differences of charge and ionic radii of Bi/Pb; elastic deformation and problem of charge compensation phenomena when x becomes higher than 0.3, inducing destabilization of the perovskite.

For $x \leq 0.075$, x-ray diagrams can be refined using $R3c$ BFO structural model with good agreement factors (e.g., $x=0.025$: GoF=1.35; $R_{wp}=7.12\%$; $R_{Bragg}=4.52\%$). With x increasing, rhombohedral distortion slowly decreases. Figure 1 gives also evidence of this phenomenon: rhombohedral splitting of peaks decrease with increasing Pb content. For highest x Pb compositions, this distortion continues to decrease until the point where the structure becomes cubic for $x>0.15$, then characterized by single and sharp reflections. Rietveld refinements performed for $x=0.20$, confirm the $Pm\bar{3}m$ space group with very good agreement factors (GoF=1.22; $R_{wp}=6.34\%$; $R_{Bragg}=4.19\%$).

Furthermore, our study points out that the rhombohedral-cubic phase transition is a first-order character, occurring with a mixture of both adjacent phases for intermediate chemical compositions $0.075<x<0.15$. Enlargement of the

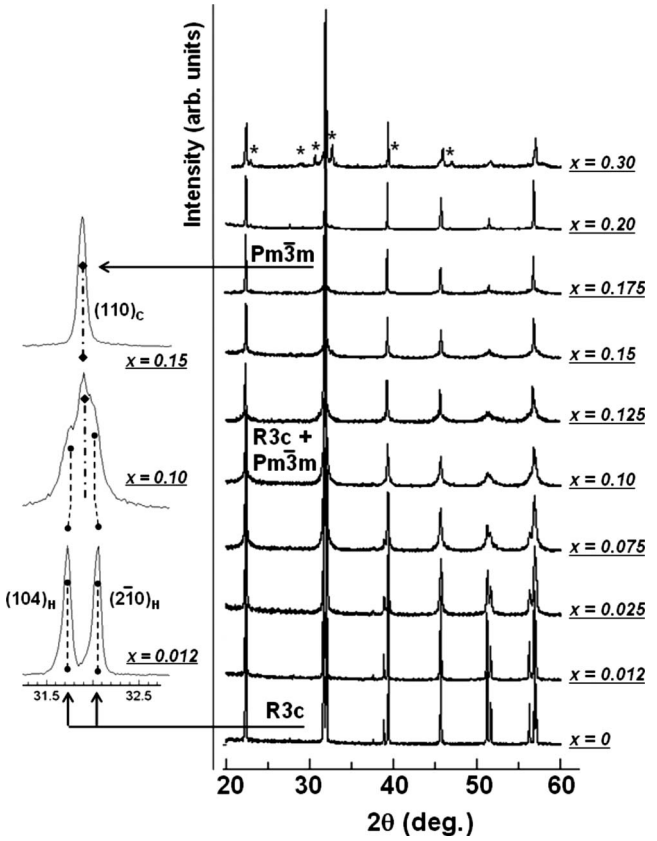

FIG. 1. X-ray diffraction patterns at room temperature for concentrations from $x=0$ to $x=0.30$.

$x=0.10$ diffraction pattern (inset of Fig. 1) clearly evidences two rhombohedral $(104)/(2\bar{1}0)$ components in coexistence with the (110) cubic one and for that reason, the peaks are widened in this region of compositions. Annealing treatments were performed on samples but have not changed the rhombohedral/cubic phases ratio, showing that this phase coexistence is an intrinsic characteristic of this system.

Table I summarizes cell parameters of rhombohedral and cubic phases, respectively, according to the chemical Pb content, the composition $x \approx 0.10$ indicates the chemical limit below or above which rhombohedral and cubic phases represent the room-temperature ground state, respectively. Interestingly, it highlights a ferroelectric-paraelectric chemically driven transition at room temperature in $Bi_{1-x}Pb_xFeO_3$.

B. Long-range order versus temperature

To characterize the stability of the ferroelectric ground state, we have performed XRD versus temperature for all the compositions $0 \leq x \leq 0.20$ reported in the Table I. According to the Bi/Pb ratio, we have observed three different temperature behaviors. Figures 2(a)–2(c) illustrate examples of patterns for each one with the associated lattice parameters evolution in Figs. 2(d)–2(f).

For the low Pb concentration region, whose ground state is ferroelectric $R3c$, the structure undergoes a structural transition toward the cubic phase with the temperature. Figure 2(a) shows the diffraction pattern obtained around the

TABLE I. Rhombohedral (a_{pc}, c_{pc}) and cubic (a_c) cell parameters for $Bi_{1-x}Pb_xFeO_3$ solid solution and critical temperatures. Rhombohedral cell parameters are expressed in the pseudocubic cell: $a_{pc}=a_H/\sqrt{2}$; $c_{pc}=c_H/2\sqrt{3}$.

$Bi_{1-x}pb_xFeO_3$	Rhombohedral phase		Cubic phase	Critical temperatures	
Pb content	a_{pc} (Å)	c_{pc} (Å)	a_c (Å)	T_C/T_m (°C)	T_f (°C)
$x=0$ (BFO)	3.9438(5)	4.0021(7)		820	725
$x=0.025$	3.9427(4)	4.0006(6)		775	625
$x=0.050$	3.9439(6)	3.9990(8)		760	575
$x=0.075$	3.9466(5)	4.0003(7)	3.9608(7)	750	350
$x=0.100$	3.9686(6)	3.9653(9)	3.9607(5)	580	300
$x=0.125$			3.9610(4)	575	250
$x=0.150$			3.9633(2)	580	240
$x=0.175$			3.9657(4)	590	
$x=0.200$			3.9644(3)		

pseudocubic reflection (110) versus the temperature for $x=0.025$. We observed that the rhombohedral distortion decreases and some reflections in other parts of the patterns disappear at the ferroelectric-paraelectric transition. Analyses of several peaks allow us to plot the temperature dependence of cell parameters for $x=0.025$ and $x=0.05$ [see Fig. 2(d)]. Evolution of the pure-phase $BiFeO_3$ cell parameters from Ref. 26 is also recalled in the graph. At this point it should be noted that although most of ferroelectric perovskites exhibit a cubic paraelectric ground state, BFO never becomes cubic at its Curie temperature ($T_C=820$ °C) (Refs. 26 and 27) but undergoes a first-order transition toward (on heating) a paraelectric monoclinic phase ($P2_1/m$), with antiferrodistorsive motions; this low-symmetry monoclinic seems to be due to a peculiar role of Bi lone pair.[26] However doping BFO with Pb atoms stabilizes the cubic "conventional" symmetry state, as it is observed in others lead-based perovkites PSN, PMN, PZT,…; interestingly, very few amount of lead as low as $x=0.025$ is enough to stabilize this long-range cubic state. The ferroelectric transition is also of first order with no group-subgroup relation between $R3c$ and $Pm\bar{3}m$ space groups. With substitution the Curie temperature is strongly shifted toward the low temperature ($\Delta T_C=-60$ °C between $x=0$ and $x=0.05$). Moreover, the rhombohedral distortion strongly decreases approaching T_C; indicating a first-order character less pronounced when x increases. Besides, data analysis allow us to determine a "freeze" temperature T_f ($T_f<T_C$) below which the mixing of phases $R3c+Pm\bar{3}m$ does not evolve. Values of T_C and T_f are reported in the Table I.

For intermediate chemical compositions close to $x\sim0.10$ the phase coexistence already exist at room temperature [Fig. 2(b)] and the temperature evolution is clearly associate to a first-order transition. Cooling down from high temperatures, rhombohedral phase appears in the cubic matrix at $T=T_C$. With decreasing temperature, the rhombohedral/cubic ratio increases as observed from the evolution of their respective Bragg peaks intensity. However below T_f intensities do not change (e.g., $T_f=575$ °C for $x=0.075$): this frozen situation corresponds to residual cubic phase embedded in a rhombohedral matrix, both phases with long-range order, as deduced from sharp diffraction reflections. [see inset of Figs. 1 and 2(b)]. Besides, a slight change in slope can be detected at T_f in the temperature evolution of rhombohedral parameters [see Fig. 2(e)], probably associated to relaxation of phase coexistence elastic constrains. Finally, increasing of Pb content induces a shift of T_C and T_f toward the low temperature (see Table I). X-ray diffraction performed with increasing and decreasing temperature also shows that mechanism described above is perfectly reversible but with a hysteresis in the characteristic temperatures. However some anomalies in full width at half maximum (FWHM), intensities and cell parameters temperature evolution point the need to investigate the structure at a more local scale, in particular, in the temperature region of the ($R3c+Pm\bar{3}m$) phase coexistence.

Similarly, for highest Pb concentrations $x>0.15$, although the structure remains cubic with $Pm\bar{3}m$ space group whatever the temperature, cell parameter exhibits unusual nonlinear temperature behavior below a T_m [see Fig. 2(f)] which can be also explained by phenomenon at a local scale, by residual nanoregions of rhombohedral phases embedded in the cubic matrix (see Sec. III C).

C. Short-range order at the phase transition

The coexistence at the $R3c-Pm\bar{3}m$ transition appears to be complex in this material when examined at a local scale. This short-range order is evidenced, in particular, by strong Lorentzian components of the diffraction peaks (see inset of Fig. 3) whose temperature evolution give information about the rhombohedral and cubic nanostructure. This widening (e.g., ~0°,7° for $x=0,10$) is too important to be only explained by existence (and ordering) of oxygen vacancies due to the Bi^{3+}/Pb^{2+} uncompensated charge. We analyze, in particular, the evolution of $(200)_{pc}$ peak that is a singulet for cubic as well as for rhombohedral symmetry. The peak has been fitted with a Gaussian and a Lorentzian contributions associated, respectively, to long-range-order phases and short-range order, i.e., nanostructure. The intensity and the

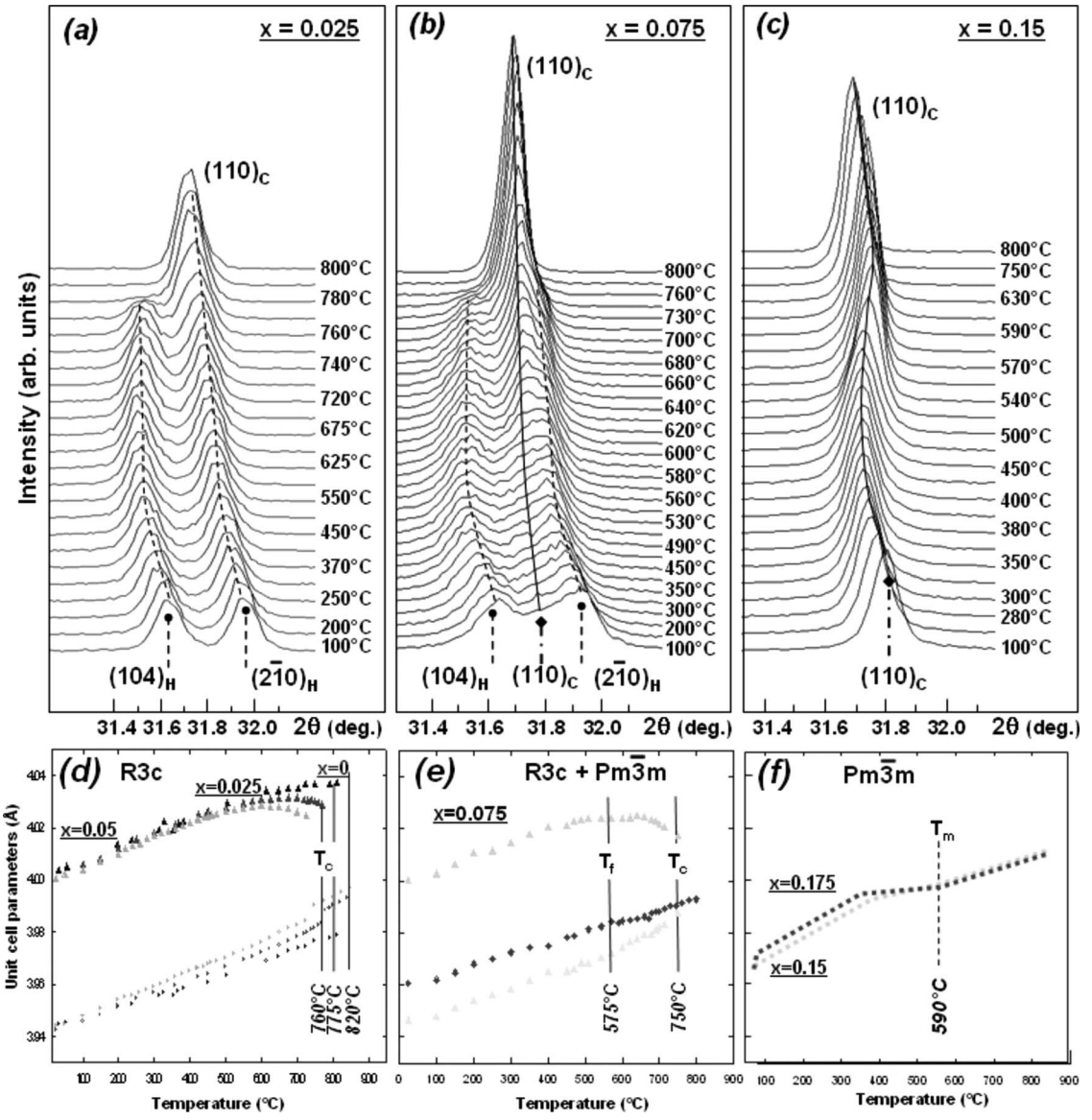

FIG. 2. Evolution of the 110_c peak for three different concentrations as a function of temperature: (a) $x=0.025$; (b) $x=0.075$; (c) $x=0.15$. Unit-cell evolution as a function of temperature for low, intermediate, and high concentrations reported in (d), (e), and (f), respectively.

width of Lorentzian component are represented as a function of concentration, at room temperature in Fig. 3. Two opposite trends are pointed out on both sides of the lead concentration $x \approx 0.10$. In particular, Fig. 3 shows that close to $x=0.10$ one passes continuously at room temperature by a progressive appearance and growth of cubic nanoregions embedded in a rhombohedral matrix (low Pb content) to an inverse situation with rhombohedral nanoregions embedded in a cubic matrix (high content of Pb); the Lorentzian component intensity is maximum for $x \approx 0.10$. Similarly, for $x < 0.10$, the FWHM of the Lorentzian contribution decreases, indicating an increasing of the coherence length of the cubic regions embedded in the rhombohedral matrix. On opposite, the FWHM decreases when $x > 0.10$: in this region, the Lorentzian contribution is assigned to the diffuse scattering associated to rhombohedral nanoregions embedded in the cubic matrix. Also, their disappearance explains the increasing of the FWHM with x Pb.

This study allow us to draw a phase diagram for the system $Bi_{1-x}Pb_xFeO_3$, displayed in Fig. 4, characterized by a huge phase coexistence, even for small concentrations of Pb. On cooling from high temperature, the first line show the temperature at which rhombohedral phase appears, either directly at long-range order in region 1 below T_C but first at short-range order in region 2. The second line drawn represents the temperature T_f below which the size of nanoregions does not evolve in the mixing of phases. This freeze temperature T_f limiting the coexistence between the two phases could have been dependent of the thermal history of the sample, as a possible kinetic of the phase coexistence could happens; this is observed, for instance, in some martensitic compounds. However we have performed x-ray experiments

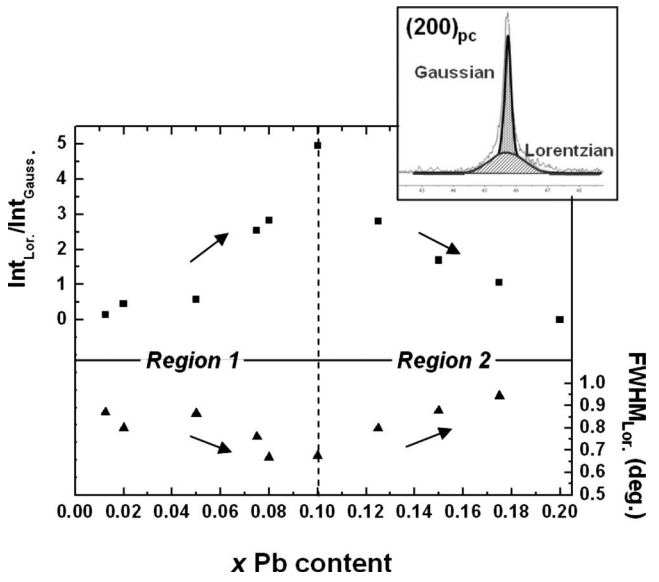

FIG. 3. Intensity (Int) and FWHM evolution of the Lorentzian part of the $(200)_{pc}$ reflection at room temperature with respect to lead doping. A deconvolution of the peak with Gaussian (Gauss.) and Lorentzian (Lor.) contributions is represented in inset.

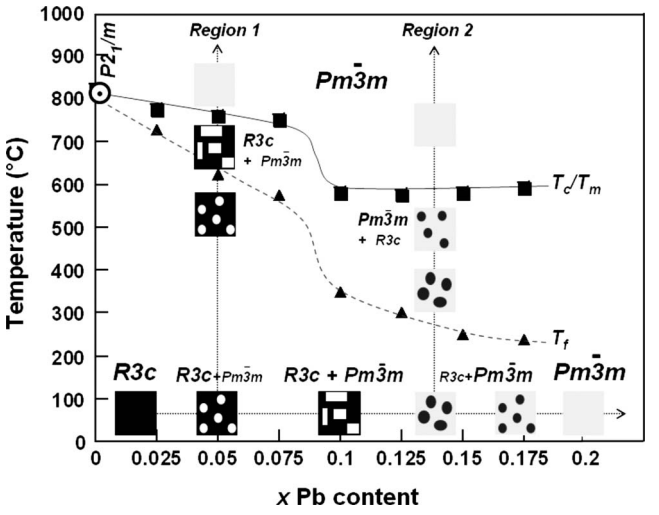

FIG. 4. Phases diagram of $Bi_{(1-x)}Pb_xFeO_3$ showing the competition between long- and short-range orders. Dark and light regions represent rhombohedral and cubic phases, respectively. Squares and triangles represent critical T_C/T_m and T_f temperatures, respectively. A schematic representation of the microstructure is proposed by circular (short-range order) and rectangular (long-range order) regions.

with different cooling rate, as well as experiments in which we quenched the samples at different T temperature with $T_C < T < T_f$; recording patterns versus time which are characteristics of the rhombohedral/cubic (nano)domains coexistence shows, in scale time of our experiment (few minutes), no time-dependent phenomenon.

IV. DISCUSSION AND CONCLUSION

A peculiar point associated to ferroelectricity in $BiFeO_3$ comes from stereochemically active $6s^2$ lone pair of Bi^{3+}. *Ab initio* calculations have already explained and predicted the ferroelectricity in $BiMnO_3$;[11] hybridization of Bi $6s$ with O $2p$ is very strong and induces a strong off-centered shift of Bi, thus a local dipole moment. Correlation of these moments induces a long-range ferroelectric order in respect with a rhombohedral symmetry and favorably energetic. Besides, temperatures of ferroelectric transition are often higher in Bi-based systems in comparison with those measured in other ferroelectrics.[28]

Although Ti ion plays the key role in the mechanism of the ferroelectricity in $BaTiO_3$, it has been also demonstrated that the lone pair of Pb^{2+} also play a dominant role in $PbTiO_3$.[29,30] Therefore lead atom gets a lone pair and is commonly understood as having a ferroelectric character, we report in this paper that adding of lead atom in the Bi subsystem of $BiFeO_3$, destroys the long-range FE order induced by Bi lone pairs on contrary. In others worlds, we do not observe a "common" ordering of the Bi and Pb lone pairs. Hybridizations of Bi-O and Pb-O and thus Bi and Pb off-centered shifts are not correlated at long range. In fact, addition of x Pb in $Bi_{1-x}Pb_xFeO_3$ progressively breaks the ferroelectric ordering up to the point where the structure becomes cubic on average. The decreasing of T_c with increasing Pb content also confirms that adding of Pb atoms destabilizes the ferroelectric rhombohedral order and stabilizes the cubic phase via a complex texture of mixed phases. Using transmission electronic microscopy as local probe (in progress), the existence of such nanostructure should be confirmed.

In the light of the literature, we believe that this mechanism can be generalized to other $(BiA)FeO_3$ solid solutions (A=Sr, La, Ca, Ba,…). Indeed, many papers reports that with increasing A content, the rhombohedral $BiFeO_3$ distortion decreases up to reach a pseudocubic cell.[13,14,31,32] Introduction of a foreign cation A disturbs the subnetwork of Bi and inhibits a ferroelectric state to develop in a long-range order in the material. In the case when A possesses a lone pair, neither competitive interaction nor correlation with the *Bi* lone pairs is observed; the ground state is finally cubic for high content of A cations. Interestingly in $Bi_{1-x}Pb_xFeO_3$, the peculiar first-order transition occurring within the whole range of chemical composition points some similarities with martensiticlike phase transitions also observed in some oxides,[33] due to the huge phase coexistence as well as in lead-based relaxor compounds, with the existence of local polar order within a paraelectric matrix.

[1] G. Smolenskii and L. E. Chupis, Sov. Phys. Usp. **25**, 475 (1982).
[2] M. Fiebig, T. Lottermoser, D. Fröhlich, A. V. Goltsev, and R. V. Pisarev, Nature (London) **419**, 818 (2002).
[3] T. Kimura, S. Kawamoto, I. Yamada, M. Azuma, M. Takano, and Y. Tokura, Phys. Rev. B **67**, 180401(R) (2003).
[4] M. Fiebig, J. Phys. D **38**, R123 (2005).
[5] M. Fiebig, Phase Transitions **79**, 947 (2006).
[6] H. Bea, M. Gajek, M. Bibes, and A. Barthelemy, J. Phys.: Condens. Matter **20**, 434221 (2008).
[7] P. Fischer, M. Polomska, I. Sosnowska, and M. Szymanski, J. Phys. C **13**, 1931 (1980).
[8] J. R. Teague, R. Gerson, and W. J. James, Solid State Commun. **8**, 1073 (1970).
[9] F. Kubel and H. Schmid, Acta Crystallogr., Sect. B: Struct. Sci. **46**, 698 (1990).
[10] A. M. Glazer, Acta Crystallogr., Sect. B Struct. Crystallogr. Cryst. Chem. **28**, 3384 (1972).
[11] N. A. Hill, J. Phys. Chem. B **104**, 6694 (2000).
[12] C. Ederer, N. A. Spaldin, Phys. Rev. B **71**, 060401(R) (2005).
[13] V. A. Khomchenko, D. A. Kiselev, E. K. Selezneva, J. M. Vieira, A. M. L. Lopes, Y. G. Pogorelov, J. P. Araujo, and A. L. Kholkin, Mater. Lett. **62**, 1927 (2008).
[14] V. A. Khomchenko, D. A. Kiselev, M. Kopcewicz, M. Maglione, V. V. Shvartsman, P. Borisov, W. Kleemann, A. M. L. Lopes, Y. G. Pogorelov, J. P. Araujo, R. M. Rubinger, N. A. Sobolev, J. M. Vieira, and A. L. Kholkin, J. Magn. Magn. Mater. (to be published).
[15] G. L. Yuan and S. W. Or, J. Appl. Phys. **100**, 024109 (2006).
[16] V. R. Palkar, D. C. Kundaliya, S. K. Malik, and S. Bhattacharya, Phys. Rev. B **69**, 212102 (2004).
[17] S. A. Ivanov, P. Nordblad, R. Tellgren, T. Ericsson, S. K. Korchagina, L. F. Rybakova, and A. Hewat, Solid State Sci. **10**, 1875 (2008).
[18] J. F. Scott, J. Phys.: Condens. Matter **20**, 021001 (2008).
[19] C. Malibert, B. Dkhil, J. M. Kiat, D. Durand, J. F. Bérar, and A. Spasojevic-de-Biré, J. Phys.: Condens. Matter **9**, 7485 (1997).
[20] D. L. Corker, A. M. Glazer, R. W. Watmore, A. Stallard, and F. Fauth, J. Phys.: Condens. Matter **10**, 6251 (1998).
[21] B. Dkhil, J. M. Kiat, G. Calvarin, G. Baldinozzi, S. B. Vakhrushev, and E. Suard, Phys. Rev. B **65**, 024104 (2001).
[22] B. Noheda, D. E. Cox, G. Shirane, R. Guo, B. Jones, and L. E. Cross, Phys. Rev. B **63**, 014103 (2000).
[23] R. Haumont, A. Al-Barakaty, B. Dkhil, J. M. Kiat, and L. Bellaiche, Phys. Rev. B **71**, 104106 (2005).
[24] V. V. Shvartsman, W. Kleemann, R. Haumont, and J. Kreisel, Appl. Phys. Lett. **90**, 172115 (2007).
[25] J. F. Bérar and P. Lelann, J. Appl. Crystallogr. **24**, 1 (1991).
[26] R. Haumont, I. A. Kornev, S. Lisenkov, L. Bellaiche, J. Kreisel, and B. Dkhil, Phys. Rev. B **78**, 134108 (2008).
[27] D. C. Arnold, K. S. Knight, F. D. Morrison, and P. Lightfoot, Phys. Rev. Lett. **102**, 027602 (2009).
[28] J. Iniguez, D. Vanderbilt, and L. Bellaiche, Phys. Rev. B **67**, 224107 (2003).
[29] R. E. Cohen, Nature (London) **136**, 358 (1992).
[30] Z. Wu and R. E. Cohen, Phys. Rev. Lett. **95**, 037601 (2005).
[31] D. H. Wang, W. C. Goh, N. Ming, and C. K. Ong, Appl. Phys. Lett. **88**, 212907 (2006).
[32] I. Sosnowska, R. Przeniosto, P. Fischer, and V. A. Murashov, J. Magn. Magn. Mater. **160**, 384 (1996).
[33] J. M. Kiat, G. Calvarin, and Y. Yamada, Phys. Rev. B **48**, 34 (1993).